Journal of Science: Advanced Materials and Devices 8 (2023) 100562

Contents lists available at ScienceDirect

Journal of Science: Advanced Materials and Devices

journal homepage: www.elsevier.com/locate/jsamd

Original Article

Miniaturized multisensor system with a thermal gradient: Performance beyond the calibration range

Matteo Tonezzer [a, b, *, 1], Luca Masera [c, 1], Nguyen Xuan Thai [d, e], Hugo Nguyen [f], Nguyen Van Duy [d, **], Nguyen Duc Hoa [d]

[a] Department of Chemical and Geological Sciences, Università di Cagliari, Campus di Monserrato, 09042 Monserrato (CA), Italy
[b] Center Agriculture Food Environment, University of Trento/Fondazione Edmund Mach, Via E. Mach 1, 38010 San Michele All'Adige, Italy
[c] DISI, University of Trento, Via Sommarive 9, Povo, Trento, Italy
[d] ITIMS, Hanoi University of Science and Technology, Hanoi, Viet Nam
[e] Vietnam Metrology Institute, 8 Hoang Quoc Viet Road, Hanoi, Viet Nam
[f] Uppsala University, Department of Materials Science and Engineering, Uppsala, Sweden

ARTICLE INFO

Article history:
Received 4 January 2023
Received in revised form
2 March 2023
Accepted 13 April 2023
Available online 18 April 2023

Keywords:
Gas sensor
Nanowire
Tin oxide
Metal decoration
Selectivity
Calibration

ABSTRACT

Two microchips, each with four identical microstructured sensors using SnO_2 nanowires as sensing material (one chip decorated with Ag nanoparticles, the other with Pt nanoparticles), were used as a nano-electronic nose to distinguish five different gases and estimate their concentrations. This innovative approach uses identical sensors working at different operating temperatures thanks to the thermal gradient created by an integrated microheater. A system with in-house developed hardware and software was used to collect signals from the eight sensors and combine them into eight-dimensional data vectors. These vectors were processed with a support vector machine allowing for qualitative and quantitative discrimination of all gases after calibration. The system worked perfectly within the calibrated range (100% correct classification, 6.9% average error on concentration value). This work focuses on minimizing the number of points needed for calibration while maintaining good sensor performance, both for classification and error in estimating concentration. Therefore, the calibration range (in terms of gas concentration) was gradually reduced and further tests were performed with concentrations outside these new reduced limits. Although with only a few training points, down to just two per gas, the system performed well with 96% correct classifications and 31.7% average error for the gases at concentrations up to 25 times higher than its calibration range. At very low concentrations, down to 20 times lower than the calibration range, the system worked less well, with 93% correct classifications and 38.6% average error, probably due to proximity to the limit of detection of the sensors.

1. Introduction

The state of lock-down due to the Covid-19 outbreak during the first half of 2020 that has brought much cleaner air and water to many countries, once again clearly demonstrated that the rapid industrialization and urbanization cause environmental problems. It is not only the global pollution that drives climate change, but also the local pollution that affects people's breathing, both outdoor and indoor, and therefore their health.

Monitoring gaseous components in air is increasingly important for many purposes, such as medical diagnosis [1], quality control of food [2], monitoring of industrial and agricultural processes [3] and security against terrorism [4], among others. Quick detection and precise estimation of different gases have always been a goal for research in the gas sensor field. Making the system affordable and portable is another important goal that is difficult to reconcile with performance. Microstructured sensors using metal oxide semiconductors (MOS) have been intensively investigated and developed in the last decades, showing their potential for these goals [5]. The main properties of MOS as sensing materials are high

* Corresponding authors. Department of Chemical and Geological Sciences, Università di Cagliari, Campus di Monserrato, 09042 Monserrato (CA), Italy.
** Corresponding author.
E-mail addresses: matteo.tonezzer@cnr.it (M. Tonezzer), nguyenvanduy@itims.edu.vn (N.V. Duy).
Peer review under responsibility of Vietnam National University, Hanoi.
[1] These authors contributed equally to the work.

https://doi.org/10.1016/j.jsamd.2023.100562

sensitivity and stability. Other important properties are low cost of fabrication, low power consumption and tiny size, making them suitable for integration into small portable devices such as smartphones, or even into wearable devices.

After first being based on thick and then thin films, the latest generation of MOS gas sensors is based on nanostructures for the purpose of improving their performance. Nanowires (NWs) are the most used nanostructures because of their good physical and chemical properties [6,7]. The sensing properties of MOS nanostructures can be tuned by controlling their size and shape [8–10]. However, resistive sensors based on MOS have two intrinsic drawbacks: high working temperature (typically higher than 200 °C) and poor selectivity. The former issue can generally be mitigated in two ways: decorating the surface of the MOS nanostructures with metallic nanoparticles (NPs), or integrating a micro-heater onto the sensor chip. The decorated catalytic metal NPs increase the sensing properties of the MOS nanomaterial, allowing it to be used at a lower operating temperature [11,12], while an on-chip integrated micro-heater greatly reduces the power consumption. The latter issue can be overcome by combining the sensors made of different MOS in arrays like in an *electronic nose* [13,14]. Electronic noses have recntly drawn large attention in the scientific literature [15,16], but their size, cost and complexity (each material requires different connectors and specific working conditions) are significantly larger than those of gas sensing systems based on a single MOS sensing material.

For this reason, we have recently proposed an alternative to electronic noses consisting of identical sensors made of the same nanomaterial but working at different temperatures [17]. We have tested different configurations in which the thermal gradient can be temporal (different responses obtained from the same sensor at different powers, sequentially) [18] or spatial (several responses obtained simultaneously, as in traditional electronic noses) [19]. Obviously, several sensors working in parallel make the measurements much faster and suitable for real-time applications. This sort of “simplified electronic nose” balances the simplicity and affordability of a MOS chemiresistor with the selectivity of a traditional electronic nose.

In this work, two multisensor chips based on a single MOS (SnO_2) NWs are used, one decorated with Ag NPs and the other with Pt NPs. Each chip consists of four resistive sensors and an integrated micro-heater and can work similarly to an electronic nose. Unlike the pioneering works of Sysoev [20,21], this innovative design (Fig. S1, Supplementary Material) is enabled by an integrated point heater that provides the thermal gradient and nanostructured materials that enhance the response intensity.

Furthermore, support vector machine (SVM) algorithms are used in this work as the core of the measurement system to provide classification and quantitative estimation of the measured gases. The performance of this type of miniaturized device within its calibration range has already proved very good (perfect classification, average error of 14.3%) [17].

On the other hand, minimizing the number of measurements required for calibration is very important for manufacturing companies. Therefore, in this work, the system performance was studied while reducing the calibration interval in order to understand how many training points are needed and how well the system works far from the calibration range.

2. Experimental

2.1. Fabrication of the sensors with on-chip synthesized SnO_2 NWs

The sensors were fabricated using an *on-chip* approach, described in detail in [17] and summarized here: first, multilayered electrodes and heater were patterned using standard UV photolithography and sputtering. Fig. 1 shows an image of the center of the sensor chip seen through an optical microscope. In this design, the heater is the tiny meander indicated by the dark red arrow, while the four sensors are shown inside the dark red-red-orange-yellow squares, indicating decreasing temperature.

The darker parts in Fig. 1 are the glass substrate, while the brighter parts are the heater and the sensor electrodes, consisting of (from bottom to top) Cr/Pt/Au/ITO layers with thicknesses of 5/80/5/20 nm, respectively. The Au layer acts as a seeding catalyst for the growth of the SnO_2 NWs, while the ITO at the top prevents the growth of NWs upwards, thus forcing them to sprout from the edges of the electrodes.

The whole sensing system including the heater and the four sensors is about $100 \times 300\ \mu m^2$. The heater, the electrodes and the distances of the sensors from the heater were optimized using COMSOL Multiphysics® simulations (Fig. S1, Supplementary Material).

Once the metal contacts were patterned, the device was inserted into a horizontal quartz tube furnace to grow the SnO_2 NWs by chemical vapor deposition (CVD). The patterned substrate was positioned on top of an alumina boat with Sn powder (purity 99.9%) and the temperature was increased to 750 °C while nitrogen was flowing. This maximum temperature was then kept for 10 min with an oxygen flow of 400 sccm, then the furnace was switched off for cooling down naturally.

The surface decoration of the SnO_2 NWs with silver and platinum nanoparticles was achieved by sputtering at a power of 10 W for 40 and 60 s, respectively. The sputtering was followed by an annealing at 600 °C in air for 4 h in order to improve the contact between the NPs and the NWs, and to stabilize the nanomaterial.

2.2. Nanomaterial characterization

Structure, morphology and composition of the metal-decorated NWs were examined by X-ray diffraction (XRD, CuK_α), field-emission scanning electron microscopy (FE-SEM, Hitachi, S-4800), Energy-dispersive X-ray spectroscopy (EDX), and transmission electron microscopy (TEM, Philips, CM 200).

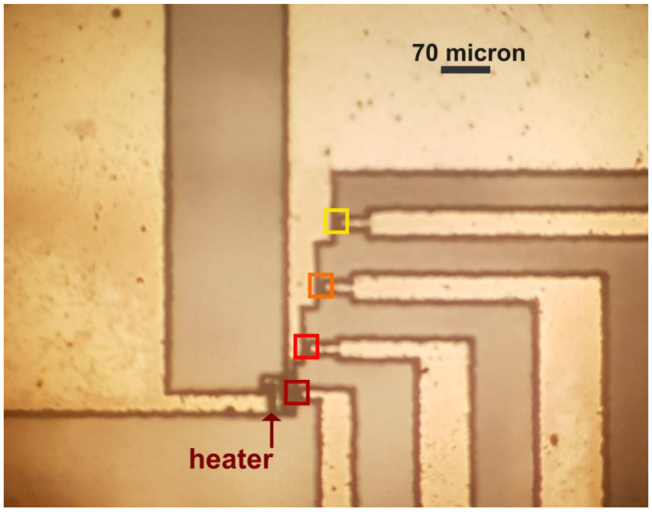

Fig. 1. Optical microscope image of a multisensor chip. The bright patterns are the heater (dark red arrow) and the sensor electrodes (inside the squares). The darker areas are the substrate.

2.3. Gas sensors measurements

The two multisensor chips, one decorated with Ag NPs and one with Pt NPs, were connected to an Arduino Mega 2560 microcontroller board. The board with a mounted sensor chip is shown in Fig. S2, where a pen also is visible for comparison of their small sizes.

The sensing system was dynamically tested with different gases (acetone, ammonia, ethanol, hydrogen and hydrogen sulfide) diluted with dry air for different concentrations. The concentration range for each gas was chosen so that it includes the strictest exposure limit value set by American institutions [22], as can be seen in Table 1.

Since all five gases tested are reducing, the sensor response in this paper is defined as $S=R_a/R_g$, where R_a is the sensor resistance in air and R_g is the resistance in the presence of the target gas.

2.4. Classification and quantification with machine learning algorithms

The eight response values from the resistive sensors were combined in one single 8-dimensional (8D) point (vector). Principal component analysis (PCA) was used to reduce the eight dimensions down to three, in order to visualize the points qualitatively [23]. Notably, this algorithm was used only to help the reader to understand the relations between the points from the different gases, while the algorithms used all the eight original dimensions to classify and quantify the gases.

The classification was performed by a support vector classifier (SVC) [24,25], while the quantification was carried out by a support vector regressor (SVR) [26,27]. Both methods, which are attracting a growing interest in the field of sensors, pertain to support vector machines [28–31] and are *supervised methods*. This means that the algorithms need a first set of data (in this case 8D vectors consisting in eight response values with two labels: gas and concentration) in order to develop a model, which then is used to compare the new unlabeled data and classify/quantify them. The concentrations used to train the multisensor system and to test its performance are shown in Table 2.

Initially, the concentrations were used alternately (starting from the extremes) to train and test the system, in order to study its sensing performance within the calibration range (see section 3.4 and Table S0 in Supplementary Material).

To test the system beyond the calibration range (at higher and lower concentrations) the configurations shown in Tables S1–7 and S8–11 in Supplementary Material were used (see further in section 3.5 and 3.6).

The Python code used to obtain the gas classification and concentration estimate is provided at the end of the Supporting Material.

3. Results and discussion

3.1. Material characterization of Ag- and Pt-decorated SnO_2 NWs

Typical SEM images of the Ag-decorated NWs are shown in Fig. 2a and b. As can be seen in Fig. 2a (low magnification), the nanowires are long, thin and smooth. Fig. 2b (high magnification) shows clearly that the Ag NPs are evenly distributed on the surface of the NWs, and this is important for their sensing properties [32,33].

The average diameter of the NWs is 94 ± 37 nm, while their average length is 38 ± 12 μm. The TEM image in Fig. 2c shows an Ag NP on the surface of a nanowire. The nanoparticle is round with a diameter of about 18 nm, while the nanowire has a diameter around 55 nm.

The EDX spectrum in Fig. S3 demonstrates that the decorated SnO_2 NWs only consist of tin, oxygen and silver. The very small amount of silver is also confirmed by XRD analysis of the same sample, as shown in Fig. S4.

Fig. 3a shows a low magnification SEM image of Pt-decorated SnO_2 NWs, while Fig. 3b shows the same at higher magnification. Also here, the Pt nanoparticles on the surface of the NWs can be seen clearly. The average length and diameter of the NWs are 35 ± 10 μm and 86 ± 32 nm, respectively, as estimated from several SEM images. As can be seen in Fig. 3b, the platinum nanoparticles are evenly distributed. Figugre 3c shows a few Pt nanoparticles on the surface of a SnO_2 nanowire.

3.2. From dynamic response to machine learning algorithms

As mentioned above, the sensor responses calculated from the raw signals (dynamic resistances) of the eight sensors (Fig. S7, Supplementary Material) were combined into 8D vectors and used as input for the machine learning algorithms. The netbook receives all the eight signals from the sensors at the same time, in parallel. Each 8D vector resumes a *thermal fingerprint* (sensor response as a function of working temperature), as previously reported in [34,35].

A first set of these 8D vectors is given to the system together with two labels: 1) the gas being measured and 2) its concentration in parts per million (ppm). These data are given to a support vector classifier with a linear kernel, acting as the brain of the sensing system. The algorithm uses this first set of labeled data to build a model (a map of the 8D space), that will be used to compare all new data and classify them. The training points pertaining to the same gas are used also to train a support vector regressor in 8D, which will be used to estimate the concentration of any new measurement, once it is classified. The construction of these models by the SVM can be considered analogous to the calibration for a traditional resistive sensor. Once the system is calibrated in this way, any new measurement data is transformed into an 8D vector without labels, which is compared with the model (8D labeled map) and classified.

Table 1
Exposure limits by the American Conference of Governmental Industrial Hygienists (ACGIH) together with the minimum and maximum concentrations tested in this paper, in parts per million.

Gas	Minimum concentration tested [parts per million]	ACGIH[a] 8-h Time Weighted Averages [parts per million]	Maximum concentration tested [parts per million]
Acetone	84	250	12,600
Ammonia	10	25	300
Ethanol	30	1000	6000
Hydrogen	10	–	400
Hydrogen sulfide	0.02	1	2.4

[a] American Conference of Governmental Industrial Hygienists (ACGIH).

Table 2
Measured concentration (used as training or testing point) for each gas.

Gas	Concentration [parts per million]									
Acetone	84	252	420	840	2520	4200	5880	8400	12,600	
Ammonia	10	30	50	70	100	150	200	250	300	
Ethanol	30	90	150	300	600	1500	2400	3000	3600	6000
Hydrogen	10	30	50	100	150	200	250	300	350	400
Hydrogen sulfide	0.02	0.04	0.1	0.2	0.4	0.8	1.4	2.0	2.4	

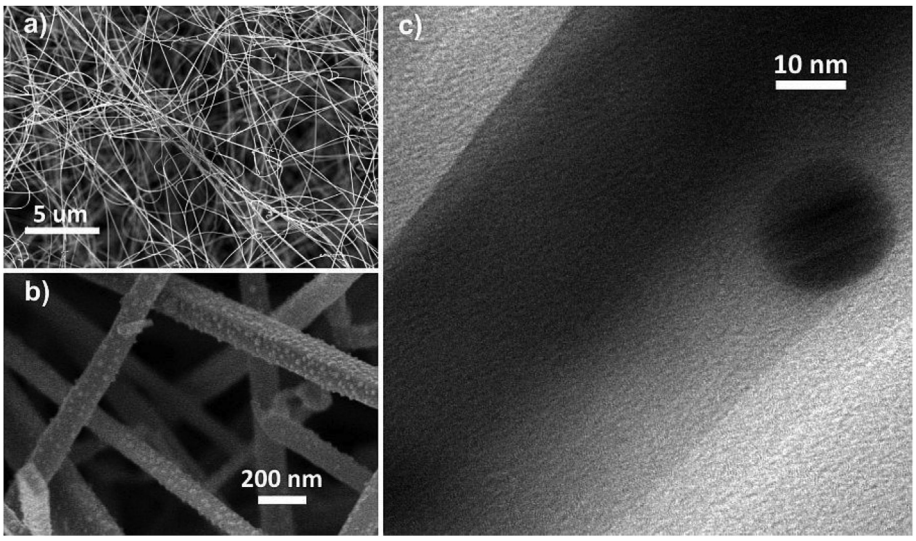

Fig. 2. a) and b) SEM images of Ag decorated SnO_2 NWs; c) TEM image of a nanowire with a silver NP on its surface.

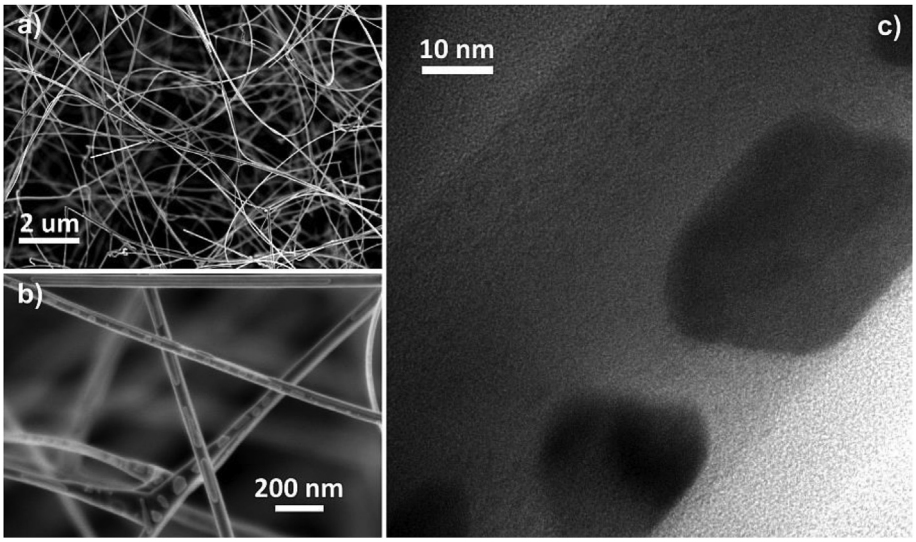

Fig. 3. a) SEM image of Pt decorated SnO_2 NWs; b) high magnification SEM image, showing the Pt nanoparticles on the NWs surface; c) TEM image of platinum NPs on a nanowire surface.

Once the new data is classified as a certain gas, the same 8D vector is also used by the regressor associated with that gas classification, in order to estimate its gas concentration.

3.3. Three-dimensional visualization with principal components analysis

Since it is impossible to see the 8D points or the model created by the support vector machine in the 8D space, PCA is used to visualize the relationships between the points coming from measurements of different gases, as shown in Fig. 4.

The PCA algorithm reduces the dimensionality of the data while keeping as much information as possible and it is attracting interest as qualitative method applied to gas sensors [36–38]. Here, PCA is used to reduce eight dimensions to three. The information contained in the first three principal components shown in Fig. 4 is very high (the sum is 91.6%), therefore the figure gives a good idea of the spatial relationships between the 8D points. As mentioned

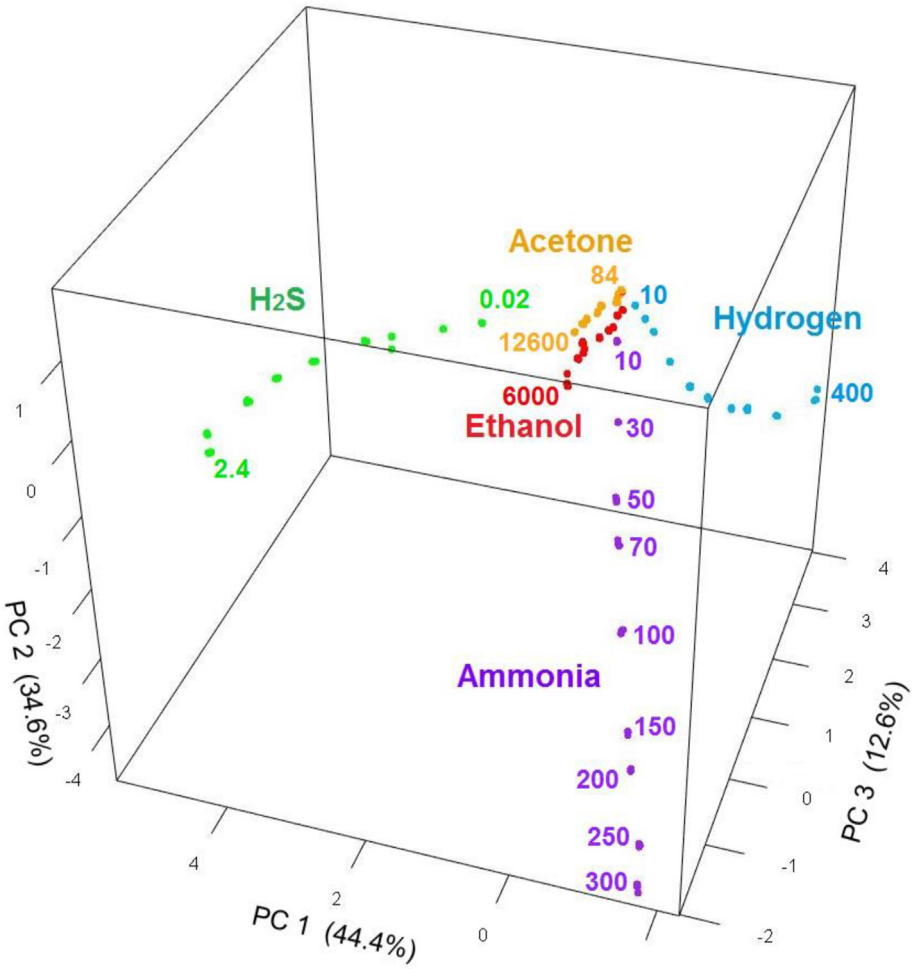

Fig. 4. PCA of the 8D data, showing the relationships between the different groups of points related to different gases.

before, this is an adaptation only for human perception, while the support vector machine fully works in 8D space, with 100% of the information.

Each point in Fig. 4 corresponds to a measurement of a certain gas at a certain concentration performed by the eight sensors simultaneously, and thus contains an entire fingerprint of the gas being measured [34,35]. Each point in Fig. 4 is colored to see to which gas it refers. The numbers in the figure represent the gas concentration in ppm. Not all values are indicated, however, due to lack of space. Each group of points relating to a gas is well separated from the others, indicating that a good classification is possible. The points relating to the gases are arranged along lines, rather than in small clouds. This does not allow the use of unsupervised distance-based methods, such as various types of clustering [39,40], forcing the use of supervised methods, and therefore a sort of calibration. On the other hand, it helps the regressor to estimate the concentration of any new measurement, as will be shown in the following sections. Fig. 4 provides some interesting observations, such as the lines from the various gases seem to lead to a common point. In fact, this common origin is pure air, to which all gases tend if extremely diluted. It should be stressed that some gases are almost overlapping close to the origin (acetone, ethanol and hydrogen), while ammonia is a little further away and hydrogen sulfide is distant from all other gases. As will be seen in the next sections, this qualitative analysis is reflected in the quantitative performance of the multisensor system.

3.4. Classification of gases and estimation of their concentration within the calibration range

As explained above, after calibration of the system with a first set of labeled data from different gases (train set), new measurements were made where the system did not know which gas it was or its concentration (test set). Using a classifier and then a regressor, the system was able to identify the gas and estimate its concentration, as reported in [20]. The classification of the multisensor system was perfect (100% of correct classifications) and the quantification was very good, with an overall error of 6.9%.

Since each gas was tested in a different concentration range according to its hazard thresholds, it is difficult to identify a common trend in a plot of error as a function of the gas concentration (Fig. S8, Supplementary Material). Therefore, in Fig. 5, the symmetric mean absolute percentage error (SMAPE) is shown as a function of the normalized concentration, i.e. the minimum train concentration for every gas becomes 0, while the maximum train concentration becomes 1. The aim is to understand if there is a trend that depends on the distance from the edges of the range on which the system was calibrated.

A U-shaped trend was expected for all gases, as the model built by the system is less robust when approaching the limits of the calibration range. Instead, an L-shaped trend was obtained, in which the error increased a lot only towards the left edge, that corresponds to low concentrations. This asymmetrical trend can be

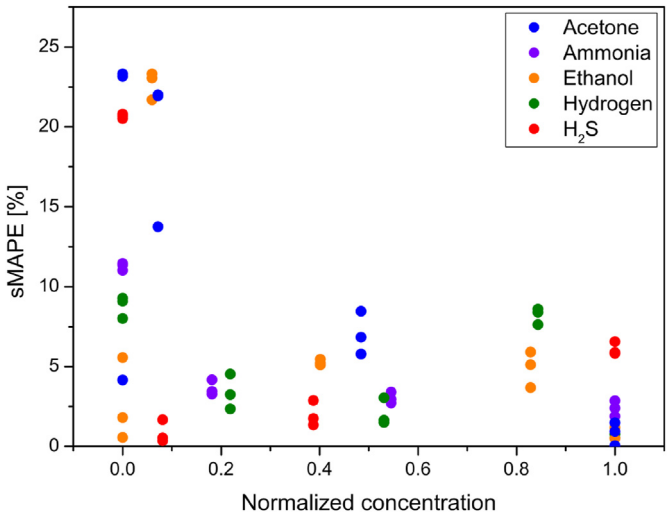

Fig. 5. Symmetric mean absolute percentage error on estimation of gas concentration as a function of the normalized gas concentration.

explained by the fact that going towards low concentrations, in addition to approaching the limit of the calibration range, the system is also approaching the limit of detection (LoD) of the sensors that compose the multisensor system.

For the points within the concentration range from >0.08 to 1.0 in Fig. 5, very low average errors for all the gases could be calculated: 3.9%, 3.0%, 3.6%, 3.5% and 3.0% for acetone, ammonia, ethanol, hydrogen and hydrogen sulfide, respectively, and 3.3% for all together. This means that the system was able to perfectly distinguish each gas (the color of each point corresponds to a specific measured gas, without any misclassification) and estimate very well its concentration.

3.5. Classification of gas and estimation of its concentration above the calibration range

The goal of this step was to test how well the multisensor system works at concentrations higher than those used for its calibration. For this purpose, we gradually reduced the upper limit of the calibration range in a series of seven experiments for each gas, according to the seven configurations in Tables S1–7 (Supplementary Material). From one configuration to the next, the calibration interval is reduced by one concentration on the right (higher concentrations), which is added to the test concentrations. The classification and quantification (error on the concentration estimate) were evaluated as a function of the distance from the calibration range.

Fig. 6 shows a confusion matrix and a graph for each of the seven configurations in Tables S1–7. The confusion matrices on the left show how well the points of the various gases were classified, and how often they were confused with other gases. The total number in each column of a confusion matrix is the number of test points for that gas. This number increases by three with each subsequent configuration. These three points are the three repetitions of the same measurement (same gas at the same concentration) that were eliminated from the calibration range and added to the test data. As can be seen, the classification is perfect for all gases in the first three configurations. In the third configuration (Tables S1–3 in Supporting Material) the maximum tested concentration is 2–4 times (depending on the gas) higher than the maximum calibration concentration. In subsequent configurations, only the classification of acetone gets worse, falling to 75 and 73.3%, then to 55.6 and finally to 28.6% in the weakest configuration (i.e. only two training points and a testing concentration 50 times larger than the maximum calibration concentration). All other gases are classified correctly, even at concentrations 60 times higher than the upper calibration limit (8, 10, 40 and 60 times higher for hydrogen, ammonia, ethanol and hydrogen sulfide, respectively). The risk for acetone to confuse with ethanol could be seen qualitatively in Fig. 4, and obviously a shorter and more distant calibration range increases the probability for misclassification.

The graphs next to the confusion matrices show the true concentration on the X axis, and the concentration estimated by the multisensor system on the Y axis. Each configuration shows three points more than the previous one, for each gas (the points taken from training and added to testing). Since the sensors are very stable and thus the results are repeatable, the points may overlap. Round colored dots indicate that the gas has been correctly classified, while crosses indicate misclassifications.

As configurations change by losing a calibration concentration (Fig. 6 a–g, corresponding to Tables S1–7 in Supplementary Material) i.e. moving the maximum calibration concentration away from the test points, the quantification gets worse.

In the last three configurations, the points at higher concentrations deviate more from the diagonal. The multisensor system obviously better quantifies measurements close to the calibration range. A reduced calibration (fewer training points) is reflected on all points, not only on the most distant ones: in Fig. 6e–g, for example, all the red points relating to H_2S deviate more and more, not only because they are further away from the trained interval, but also because the calibration is done with fewer points and is therefore less accurate.

To better understand the trend of the concentration error as a function of the configuration (i.e. the calibration range and the distance of the test points from it), the error made by the multisensor on each point is presented for each gas in Fig. 7. The seven graphs in each panel (a–e, each relating to a gas) refer to the seven configurations used (Tables S1–7, Supporting Material). Here, the vertical green lines indicate the training concentrations used to calibrate the system, and the light-green background indicate the calibration range. Test points outside the calibration interval are indicated as dots or crosses. The colored round dots indicate correctly classified points, while the crosses indicate misclassified points, in the same way as in Fig. 6. Colored dots and crosses, to be read on the left scale, indicate the symmetric absolute percentage error calculated using the gas concentration estimated by the multisensor system. Since three repetitions were made for each measurement, three symbols (which may overlap) are present at each test concentration. The black squares and lines, to be read on the right scale, are the percentage of correct classification at that test concentration.

Notably, in Fig. 7 the points of the three repetitions of each measure in some cases are quite distant from each other. This can be explained by the fact that the 8-dimensional regression greatly amplifies any small distance, although the response differences are small.

The points do not always have the same trend as the calibration range narrows and thus moves away from them. An increased error was expected as the distance increases. However, classification and regression in eight dimensions are operations that introduce random statistical errors that can be comparable or even larger than those intrinsic to the resistive sensors.

All gases show a perfect classification and a low error in the top three configurations of each panel. Four gases are correctly classified in all configurations, whereas acetone is misclassified (confused with ethanol) when the measurement is too far from the calibration interval (at a concentration three times higher than the

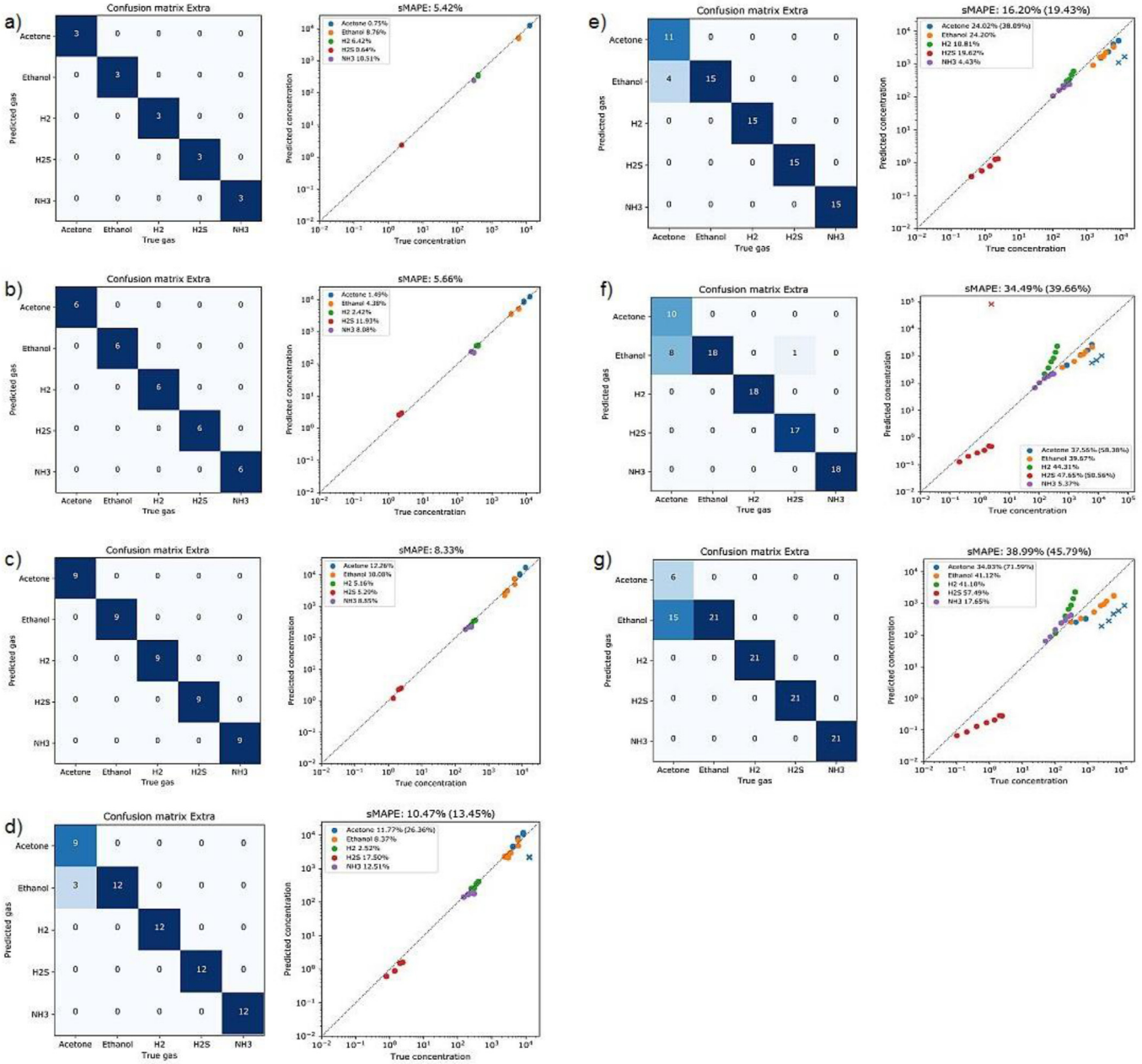

Fig. 6. Confusion matrices (left) and estimated concentrations of gases versus their true concentrations (right), corresponding to the configurations with low concentration calibration ranges (Tables S1–7 in Supplementary Material).

calibration limit). Hydrogen sulfide has a measurement incorrectly classified in the penultimate configuration, probably because of a statistical error, since only one of the three repetitions is misclassified. Nevertheless, it is correctly classified in the last configuration, albeit a more difficult condition, at a concentration of 60 times higher than the maximum calibration concentration (2.4 vs 0.04 ppm). Ammonia is correctly classified up to a concentration of 10 times higher than the upper limit of the calibration range (300 vs 30 ppm), ethanol 40 times higher (6000 vs 150 ppm) and hydrogen up to 8 times more (400 vs 40 ppm). Thus, the only gas that has classification problems is acetone when the testing points are at concentrations of ten times higher than the calibration interval (2520 vs 252 ppm).

In the final and worst configuration, the error in the concentration estimation is 34.0, 17.6, 41.1, 41.1 and 57.5% for acetone, ammonia, ethanol, hydrogen and hydrogen sulfide, respectively, for an overall error of 39.0%. However, it should be remembered that the multisensor works up to concentrations of 60 times higher than the upper calibration limit.

3.6. Classification of gas and estimation of its concentration below the trained range

The system was also tested for concentrations below the calibration range, with only four configurations (Tables S8–11, Supplementary Material) and the results are shown in Fig. 8.

The confusion matrices show that ethanol classification encounters problems already with the easiest configuration.

In the more difficult configurations, also hydrogen and ammonia are classified in part incorrectly, while acetone and hydrogen

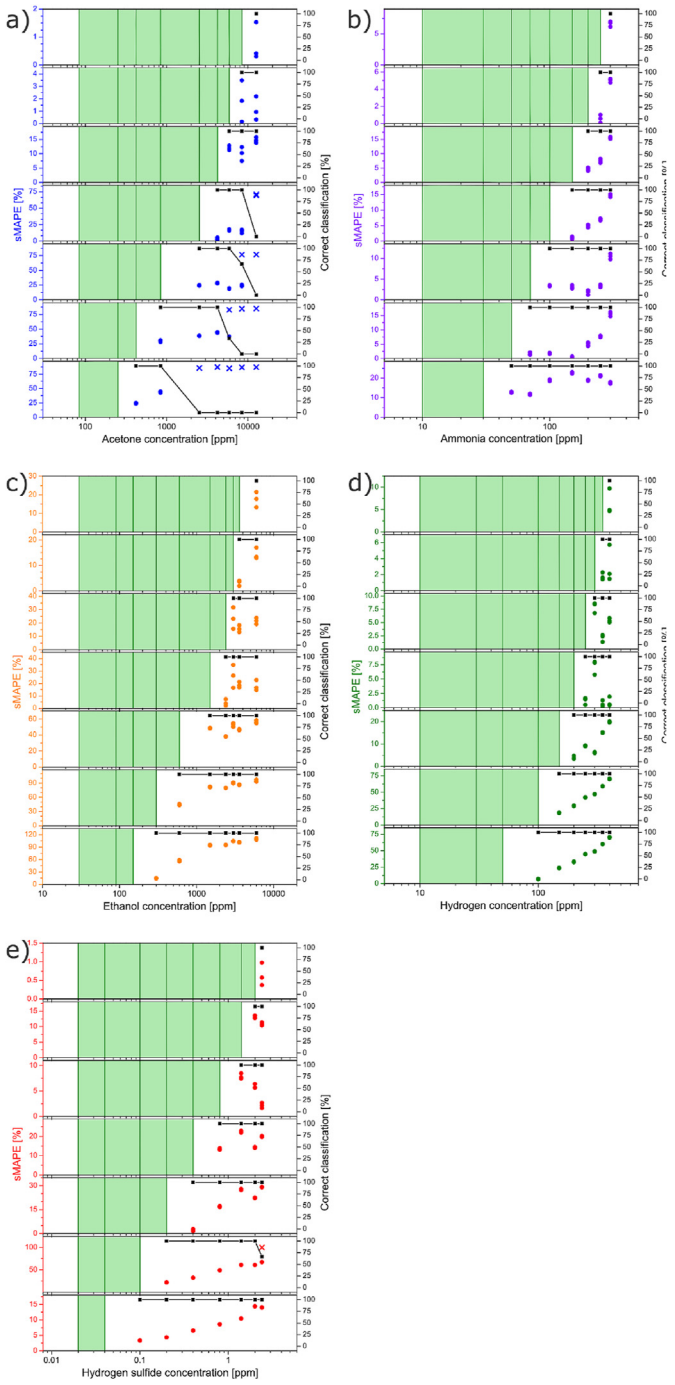

Fig. 7. Symmetric absolute percentage error of concentration estimations for each gas, as the calibration concentration range is reduced, for concentrations higher than the maximum calibration concentration.

sulfide are always classified correctly. All the misclassified gases in the four matrices are confused with acetone.

The graphs next to the confusion matrices in Fig. 8 show that many symbols are further away from the diagonal than those in the first configurations in Fig. 6, meaning that concentrations below the calibration range are more difficult to estimate than those above. This is also evident from the average error reported above each graph.

To better understand the trend of the error as a function of the configuration, the error made by the multisensor on each point is calculated and shown in Fig. 9. In many cases the error increases as the calibration range moves away from the test points. The three points for each repeated measurement seem in general reproducible (overlapping or very close to each other). The plots in Fig. 9 clearly show that the performance of the multisensor system decreases as the testing concentrations move away from the calibration interval. With the shortest and farthest training range (bottom plot in each panel, worst condition), the classification is correct in 93.3% of cases (100% for all gases, but 66.7% for ethanol).

Three gases (ammonia, ethanol and hydrogen) can be misclassified, especially at much lower concentrations than their trained range. Ethanol is always misclassified at its lowest concentration (20 times lower than the calibration range) and in one single case at 150 ppm (bottom plot of Fig. 9c, when the lowest concentration of the calibration range was 600 ppm), while hydrogen is sometimes misclassified at its lowest concentration (10 ppm). Ammonia is partially misclassified in one case at its lowest concentration (7 times lower than the calibration interval), while acetone and hydrogen sulfide are never misclassified down to their minimum test concentration, respectively of 30 and 20 times lower than the calibration range limit.

In the worst configuration (the lowest graph in each panel) 116 out of 120 points are classified correctly, for a percentage of 96.7%.

The symmetric mean absolute percentage error in this configuration is 20.4, 6.6, 16.8, 11.1 and 40.6% relatively for acetone, ammonia, ethanol, hydrogen and hydrogen sulfide without accounting for the four misclassified points (on which the error makes no sense). The average error over all gases is 19.3%.

3.7. Comparison of the concentration estimations outside the trained range

Previous sections have shown that the system classifies well the gases, both at much higher (60 times higher) and much lower (30 times lower) concentrations than the calibration limits. The estimation of the gas concentrations is also good, with a relatively small SMAPE. In both classification and quantification, the performance of the multisensor system is better at concentrations above the upper limit of the calibration range than below the lower limit.

Fig. 10 compares the extensions at lower and higher concentrations. The concentrations (x axis) were normalized to the lowest calibration concentration (in the graph on the left) and the highest (in the graph on the right) so that the gases could be compared.

Fig. 10 clearly shows that the trends on the two sides of the calibration interval are not symmetrical. On the right it tends to the expected U shape (the right half of a U), while on the left the error is larger and does not show any conceivable trend, depending more on the specific gas. This discrepancy can be explained by the intrinsic asymmetry in the response of the resistive sensors that make up the sensing system: as the distance from the lower limit of the calibration range increases (i.e. concentration goes towards zero), the multisensor system approaches the intrinsic limit of detection of the resistive sensors.

3.8. Comparison with scientific literature

A comprehensive comparison of the multisensor performance investigated here with that of the devices in the literature is difficult, since the electronic noses based on metal oxide nanowires are a recent field of study and there are still few papers reporting quantitative results [41].

However, Table 3 reports the results of the devices most similar to the multisensor fabricated and studied in this work.

The table shows that the multisensor are the best within the calibration range, but are also good outside the calibration range,

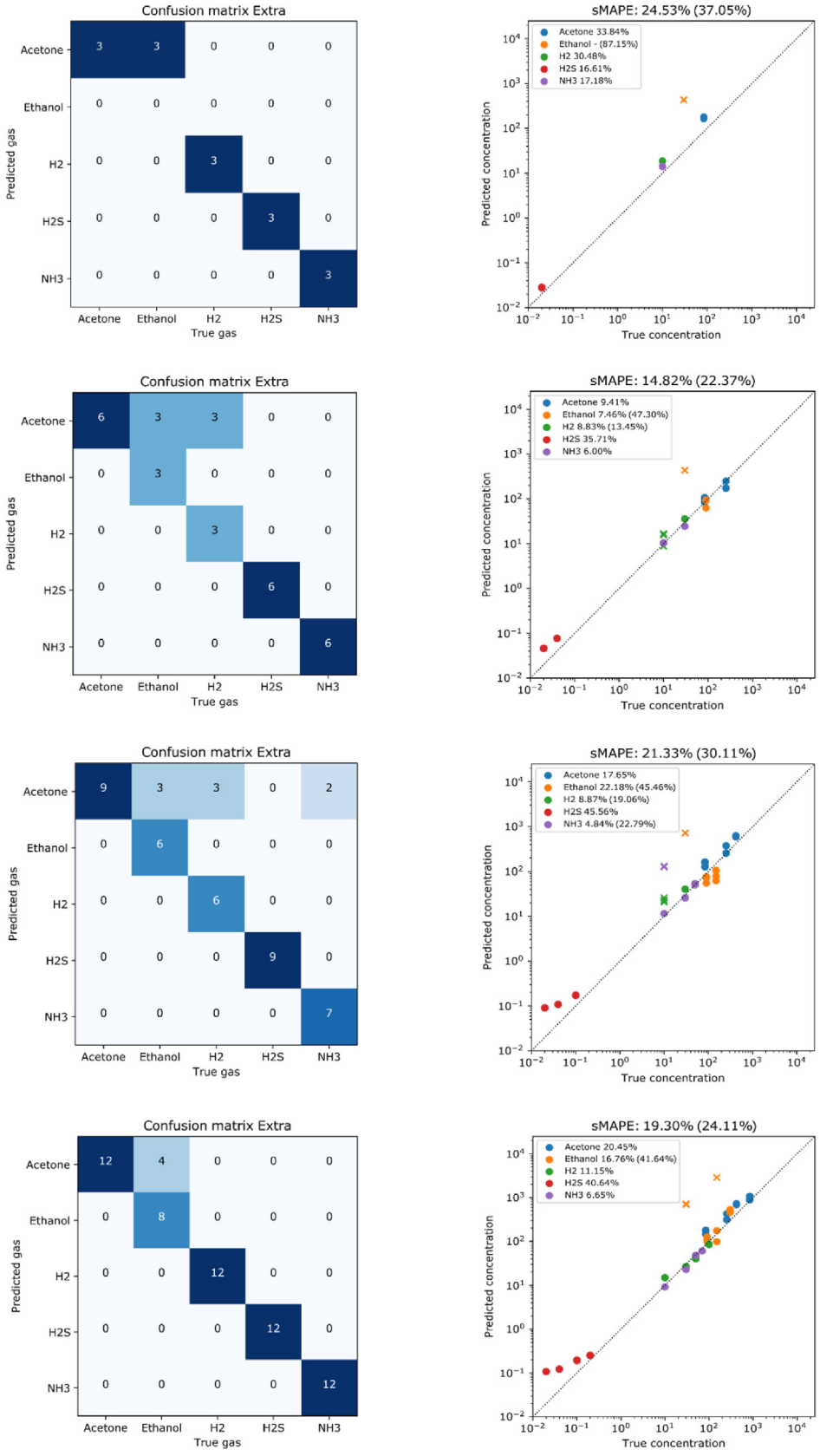

Fig. 8. Confusion matrices (left) and estimated gas concentration versus true gas concentrations (right), at concentrations lower than the calibration range.

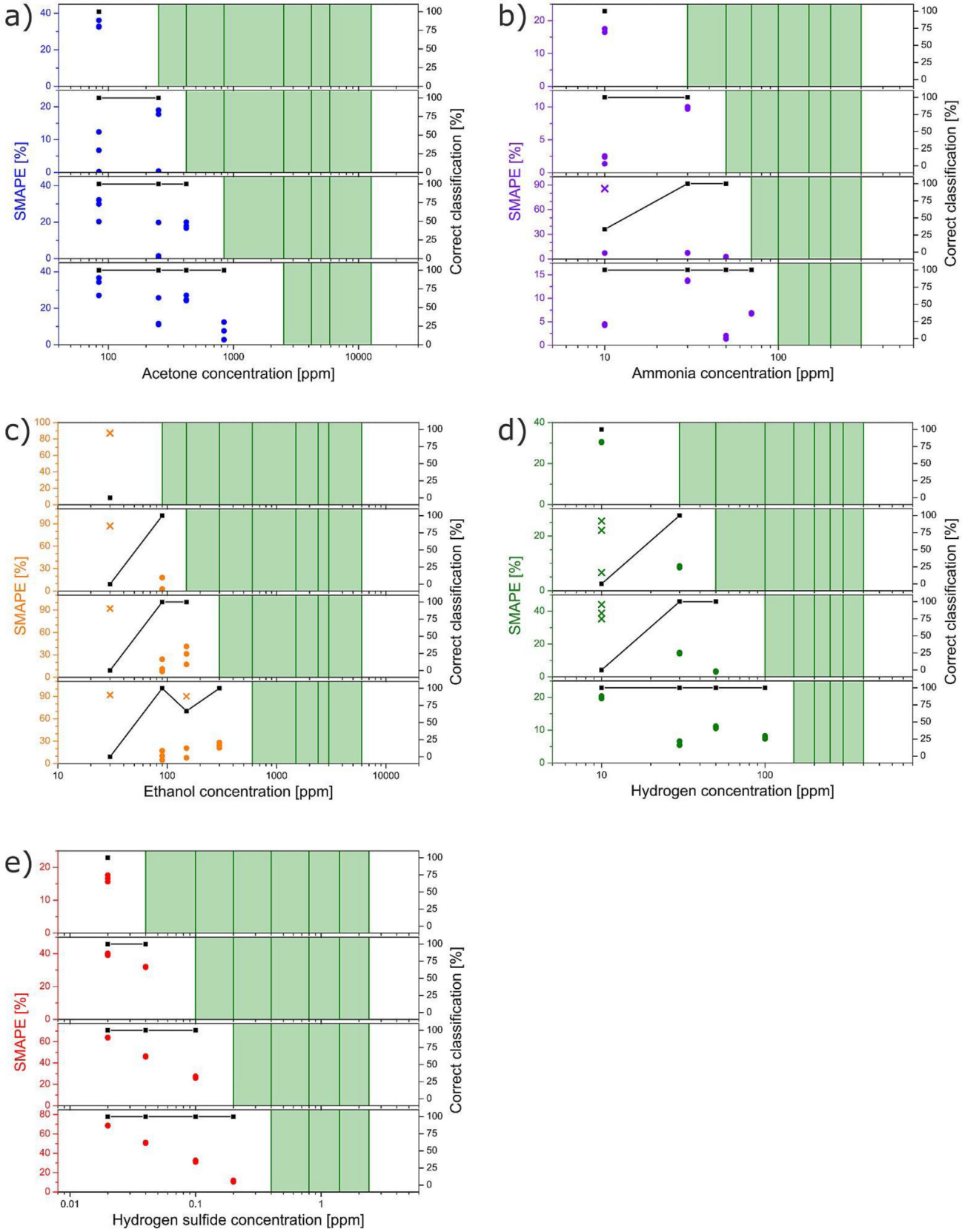

Fig. 9. Symmetric absolute percentage error of concentration estimates for each gas, as a function of the calibration concentration range and the distance from it, for concentrations lower than the minimum training concentration.

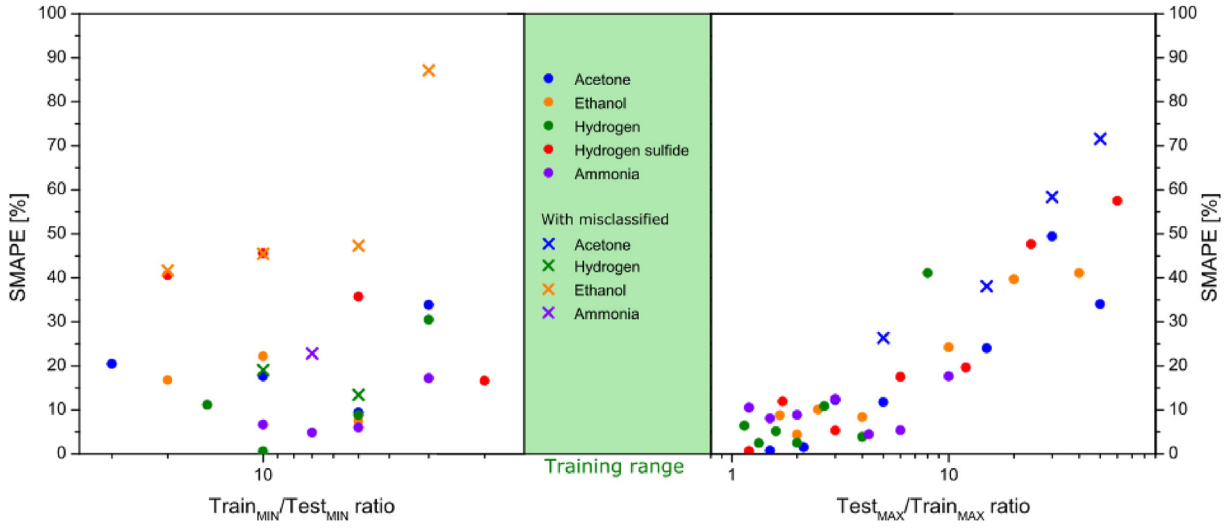

Fig. 10. Symmetric mean absolute percentage error of concentration estimates for each gas, as a function of the distance from the calibration range (normalized respectively to the lower and upper limit of the calibration interval).

Table 3
Comparison between the performance of the multisensor manufactured and those of the devices in the literature.

Materials	Gas or sample detected	Concentration (ppm)	Method	Classification (%)	Concentration error (%)	Ref.
SnO_2 + Ag, Pt	CH_3COCH_3, NH_3, H_2, H_2S, C_2H_5OH	0.02–12,600	SVM	100	14.3	[17]
SnO_2 + Ag	H_2S, H_2, NH_3, C_2H_5OH, CH_3COCH_3	0.25–10,000	SVM	100	15.3	[18]
NiO	H_2, CO, CO_2, C_2H_5OH	5–10,000	SVM	100	14.8	[19]
SnO_2 + Pt	CH_3COCH_3, benzene, C_2H_5OH, H_2, toluene	0.1–100	SVM	100	14.1	[35]
ZnO, CuO NWs + Pd, Ag	H_2, CO, NO_2	200	LDA	95	No	[42]
SnO_2	H_2, CO, NO_2, C_2H_5OH, CH_3COCH_3, NH_3, toluene	1–50	SVM	94.3	24.5	[43]
C–SnO_2	CH_3COCH_3, NH_3, CO, C_2H_5OH, H_2, toluene	1–50	KNN, Extra Trees, MLP	100	36.0	[44]
SnO_2	CH_3COCH_3, NH_3, C_2H_5OH, H_2, NO_2	5–250	SVM	100	7.6	[45]
ZnO				95	9.2	
ZnO	NH_3, CO_2, H_2S	0.5–1000	RF	99.8	No	[46]
ZnO, SnO_2, TiO_2 + Au	cheese	not applicable	PLS	82.05	not applicable	[47]
SnO_2, CuO + Au	cheese	not applicable	ANN	84.1	not applicable	[48]
SnO_2	fish, pork	not applicable	SVM	95.2	not applicable	[49]
SnO_2	chicken	not applicable	RF	95.42	not applicable	[50]
SnO_2	breath	not applicable	XGBoost	52.1	not applicable	[51]
SnO_2 + Pt, Ag	CH_3COCH_3, NH_3, C_2H_5OH, H_2, H_2S	0.02–12,600	SVM	100	6.9 (inside the calibration range)	**This work**
				96	31.7 (25 times higher than calibration)	
				93	38.6 (20 times lower than calibration)	

both at concentrations up to 25 times higher and at concentrations down to 20 times lower than the calibration interval, especially regarding gas classification.

4. Conclusions

An innovative multi-sensor system based on resistive sensors working in the thermal gradient from an integrated heater has been used. The system, consisting of two chips, each with four sensors based on metal-decorated SnO_2 nanowires, was tested to measure five reducing gases (acetone, ammonia, ethanol, hydrogen, and hydrogen sulfide). The device, completely home-made, light, and portable (smaller than a smartphone), was able to distinguish all the tested gases and estimate their concentrations. When used for measurement of concentrations within the calibration range, the system showed excellent performance with 100% correct classifications and an average concentration error of 6.9%.

The purpose of this work, however, was to find out how much the calibration range could be reduced while maintaining good sensor performance. The results showed that even after training the system with few points (down to only two points for each gas), the system worked very well with 98% correct classifications and 16.4% average error for concentrations of more than six times higher than its trained range, and with 96% correct classifications and 31.7% average error for concentrations up to 25 times higher than its calibration range. Below the calibration range, however, system performance decreases, with 93% correct classifications and 38.6% mean error up to concentrations 20 times lower than its calibration limit.

The experiments showed that with a simple and fast calibration step, the sensing system was able to classify and quantify all the tested gases over a wide range of concentrations. These results show that the miniaturized sensor system with support vector machine algorithms can be calibrated quickly with a few points but

still can provide good performance, both in terms of classification and quantification.

Data availability

The data that support the findings of this study are available within the article and its Supplementary Material.

Declaration of competing interest

The authors declare that they have no known competing financial interests or personal relationships that could have appeared to influence the work reported in this paper.

Acknowledgments

This work was funded by the European Union's Horizon 2020 research and innovation programme [grant number 101016411]. This material was also based upon the work supported by the Air Force Office of Scientific Research under Award No. FA2386- 22-1-4043. The authors acknowledge Myfab Uppsala for providing facilities and experimental support. Myfab is funded by the Swedish Research Council (2019-00207) as a national research infrastructure.

Appendix A. Supplementary data

Supplementary data to this article can be found online at https://doi.org/10.1016/j.jsamd.2023.100562.

References

[1] B. Han, J. Wang, W. Yang, X. Chen, H. Wang, J. Chen, C. Zhang, J. Sun, X. Wei, Hydrothermal synthesis of flower-like In_2O_3 as a chemiresistive isoprene sensor for breath analysis, Sens. Actuators, B 309 (2020), 127788.
[2] M. Senapati, P.P. Sahu, Meat quality assessment using Au patch electrode Ag-SnO_2/SiO_2/Si MIS capacitive gas sensor at room temperature, Food Chem. 324 (2020), 126893.
[3] T. Lin, S.B. Shah, L. Wang-Li, E.O. Oviedo-Rondón, J. Post, Development of MOS sensor-based NH_3 monitor for use in poultry houses, Comput. Electron. Agric. 127 (2016) 708.
[4] D. Wang, Y. Cheng, K. Wan, J. Yang, J. Xu, X. Wang, High efficiency xylene detection based on porous MoO3 nanosheets, Vacuum 179 (2020), 109487.
[5] R. Malik, V.K. Tomer, Y.K. Mishra, L. Lin, Functional gas sensing nanomaterials: a panoramic view, Appl. Phys. Rev. 7 (2020), 021301.
[6] A. Mirzaei, J.-H. Lee, S.M. Majhi, M. Weber, M. Bechelany, H.W. Kim, S.S. Kim, Resistive gas sensors based on metal-oxide nanowires, J. Appl. Phys. 126 (2019), 241102.
[7] V. Demontis, M. Rocci, M. Donarelli, R. Maiti, V. Zannier, F. Beltram, L. Sorba, S. Roddaro, F. Rossella, C. Baratto, Conductometric sensing with individual InAs nanowires, Sensors 19 (2019) 2994.
[8] B.-Y. Wang, D.-S. Lim, Y.-J. Oh, CO gas detection of Al-doped ZnO nanostructures with various shapes, Jpn. J. Appl. Phys. 52 (2013), 101103.
[9] M. Tonezzer, T.T.L. Dang, N. Bazzanella, V.H. Nguyen, S. Iannotta, Comparative gas-sensing performance of 1D and 2D ZnO nanostructures, Sens. Actuators, B 220 (2015) 1152.
[10] C. Baratto, Growth and properties of ZnO nanorods by RF-sputtering for detection of toxic gases, RSC Adv. 8 (2018) 32038–32043.
[11] J.-S. Lee, A. Katoch, J.-H. Kim, S.S. Kim, Effect of Au nanoparticle size on the gas-sensing performance of p-CuO nanowires, Sensor. Actuator. B Chem. 222 (2016) 307.
[12] Y. Xu, T. Ma, Y. Zhao, L. Zheng, X. Liu, J. Zhang, Multi-metal functionalized tungsten oxide nanowires enabling ultra-sensitive detection of triethylamine, Sens. Actuators, B 300 (2019), 127042.
[13] E.N. Carmona, V. Sberveglieri, A. Ponzoni, V. Galstyan, D. Zappa, A. Pulvirenti, E. Comini, Detection of food and skin pathogen microbiota by means of an electronic nose based on metal oxide chemiresistors, Sens. Actuators, B 238 (2017) 1224.
[14] P.S. Gromski, E. Correa, A.A. Vaughan, D.C. Wedge, M.L. Turner, R. Goodacre, A comparison of different chemometrics approaches for the robust classification of electronic nose data, Anal. Bioanal. Chem. 406 (2014) 7581.
[15] R. Capuano, E. Paba, A. Mansi, A.M. Marcelloni, A. Chiominto, A.R. Proietto, E. Zampetti, A. Macagnano, L. Lvova, A. Catini, R. Paolesse, G. Tranfo, C. Di Natale, Aspergillus species discrimination using a gas sensor array, Sensors 20 (2020) 4004.
[16] D. Di Giuseppe, A. Catini, E. Comini, D. Zappa, C. Di Natale, E. Martinelli, Optimizing MOX sensor array performances with a reconfigurable self-adaptive temperature modulation interface, Sens. Actuators, B 333 (2021), 129509.
[17] N.X. Thai, M. Tonezzer, L. Masera, H. Nguyen, N.V. Duy, N.D. Hoa, Multi gas sensors using one nanomaterial, temperature gradient, and machine learning algorithms for discrimination of gases and their concentration, Anal. Chim. Acta 1124 (2020) 85.
[18] T.M. Ngoc, N. Van Duy, C.M. Hung, N.D. Hoa, H. Nugyen, M. Tonezzer, N. Van Hieu, Self-heated Ag-decorated SnO_2 nanowires with low power consumption used as a predictive virtual multisensor for H_2S-selective sensing, Anal. Chim. Acta 108 (2019) 108.
[19] M. Tonezzer, D.T.T. Le, S. Iannotta, N. Van Hieu, Selective discrimination of hazardous gases using one single metal oxide resistive sensor, Sens. Actuators, B 277 (2018) 121.
[20] V.V. Sysoev, I. Kisilev, M. Frietsch, J. Goschnick, Temperature gradient effect on gas discrimination power of a metal-oxide thin-film sensor microarray, Sensors 4 (2004) 37.
[21] V.V. Sysoev, E. Strelcov, S. Kar, A. Kolmakov, The electrical characterization of a multi-electrode odor detection sensor array based on the single SnO_2 nanowire, Thin Solid Films 520 (2011) 898.
[22] https://www.osha.gov/dsg/annotated-pels/index.html.
[23] S. Xu, Z. Zhou, H. Lu, X. Luo, Y. Lan, Improved algorithms for the classification of rough rice using a bionic electronic nose based on PCA and the Wilks distribution, Sensors 14 (2014) 5486.
[24] S. Alam, S.K. Sonbhadra, S. Agarwal, P. Nagabhushan, One-class support vector classifiers: a survey, Knowl. Base Syst. 196 (2020), 105754.
[25] Y.-H. Liao, Z.-C. Wang, F.-G. Zhang, M.F. Abbod, C.-H. Shih, J.-S. Shieh, Machine learning methods applied to predict ventilator-associated pneumonia with Pseudomonas aeruginosa infection via sensor array of electronic nose in intensive care unit, Sensors 19 (2019) 1866.
[26] Y. Kang, M. Ozdogan, X. Zhu, Z. Ye, C. Hain, M. Anderson, Comparative assessment of environmental variables and machine learning algorithms for maize yield prediction in the US Midwest, Environ. Res. Lett. 15 (2020), 064005.
[27] S. Acharaya, D. Swaminathan, S. Das, K. Kansara, S. Chakraborty, D. Kumar, T. Francis, K.R. Aatre, Non-invasive estimation of hemoglobin using a multi-model stacking regressor, IEEE J. Biomed. Health 24 (2020) 1717.
[28] H. Drucker, C.J.C. Burges, L. Kaufman, A.J. Smola, V.N. Vapnik, Support vector regression machines, Adv. Neural Inf. Process. Syst. 9 (1997) 155.
[29] S. Xu, X. An, X. Qiao, L. Zhu, L. Li, Multi-output least-squares support vector regression machines, Pattern Recogn. Lett. 34 (2013) 1078.
[30] J.A.K. Suykens, J.P.L. Vandewalle, Least squares support vector machine classifiers, Neural Process. Lett. 9 (1999) 293.
[31] M.A. Almasre, H. Al-Nuaim, Comparison of four SVM classifiers used with depth sensors to recognize Arabic sign language words, Computers 6 (2020) 20.
[32] Z.U. Abideen, J.-H. Kim, S.S. Kim, Optimization of metal nanoparticle amount on SnO_2 nanowires to achieve superior gas sensing properties, Sens. Actuators, B 238 (2017) 374.
[33] J.-H. Lee, A. Mirzaei, J.-Y. Kim, J.-H. Kim, H.W. Kim, S.S. Kim, Optimization of the surface coverage of metal nanoparticles on nanowires gas sensors to achieve the optimal sensing performance, Sens. Actuators, B 302 (2020), 127196.
[34] M. Tonezzer, T.T.L. Dang, Q.H. Tran, V.H. Nguyen, S. Iannotta, Selective hydrogen sensor for liquefied petroleum gas steam reforming fuel cell systems, Int. J. Hydrogen Energy 42 (2017) 740.
[35] M. Tonezzer, J.-H. Kim, J.-H. Lee, S. Iannotta, S.S. Kim, Predictive gas sensor based on thermal fingerprints from Pt-SnO2 nanowires, Sens. Actuators, B 281 (2019) 670.
[36] M.A. Hossain Khan, B. Thomson, J. Yu, R. Debnath, A. Motayed, M.V. Rao, Scalable metal oxide functionalized GaN nanowire for precise SO_2 detection, Sens. Actuators, B 318 (2020), 128223.
[37] P. Srinivasan, J. Robinson, J. Geevaretnam, J.B.B. Rayappan, Development of electronic nose (Shrimp-Nose) for the determination of perishable quality and shelf-life of cultured Pacific white shrimp (Litopenaeus Vannamei), Sens. Actuators, B 317 (2020), 128192.
[38] M.M.O. Netto, W.B. Gonçalves, R.W.C. Li, J. Gruber, Biopolymer based ionogels as active layers in low-cost gas sensors for electronic noses, Sens. Actuators, B 315 (2020), 128025.
[39] J. Mao, Y. Lu, N. Chang, J. Yang, S. Zhang, Y. Liu, Multidimensional colorimetric sensor array for discrimination of proteins, Biosens. Bioelectron. 86 (2016) 56.
[40] M. Mahmoudi, S.E. Lohse, C.J. Murphy, K.S. Suslick, Identification of nanoparticles with a colorimetric sensor array, ACS Sens. 1 (2016) 17.
[41] M. Tonezzer, D.T.T. Le, L.V. Duy, N.D. Hoa, F. Gasperi, N.V. Duy, F. Biasioli, Electronic noses based on metal oxide nanowires: a review, Nanotechnol. Rev. 11 (2022) 897–925.
[42] Y. Hu, H. Lee, S. Kim, M. Yun, A highly selective chemical sensor array based on nanowire/nanostructure for gas identification, Sensor. Actuator. B Chem. 181 (2013) 424.
[43] M. Tonezzer, Selective gas sensor based on one single SnO_2 nanowire, Sensor. Actuator. B Chem. 288 (2019) 53.
[44] M. Tonezzer, S.C. Izidoro, J.P.A. Moraes, L.T.T. Dang, Improved gas selectivity based on carbon modified SnO2 nanowires, Front. Mater. 6 (2019) 277.

[45] M. Tonezzer, C. Armellini, L. Toniutti, Sensing performance of thermal electronic noses: a comparison between ZnO and SnO_2 nanowires, Nanomaterials 11 (2021) 2773.
[46] S. Kanaparthi, S.G. Singh, Discrimination of gases with a single chemiresistive multi-gas sensor using temperature sweeping and machine learning, Sensor. Actuator. B Chem. 348 (2021), 130725.
[47] M. Abbatangelo, E. Núñez-Carmona, V. Sberveglieri, Application of a novel S3 nanowire gas sensor device in parallel with GC-MS for the identification of Parmigiano Reggiano from US and European competitors, J. Food Eng. 236 (2018) 36.
[48] M. Abbatangelo, E. Núñez-Carmona, V. Sberveglieri, D. Zappa, E. Comini, G. Sberveglieri, Application of a novel S3 nanowire gas sensor device in parallel with GC-MS for the identification of rind percentage of grated Parmigiano Reggiano, Sensors 18 (2018) 18.
[49] M. Tonezzer, Single nanowire gas sensor able to distinguish fish and meat and evaluate their degree of freshness, Chemosensors 9 (2021) 9249.
[50] S.D. Astuti, M.H. Tamimi, A.A.S. Pradhana, K.A. Alamsyah, H. Purnobasuki, M. Khasanah, et al., Gas sensor array to classify the chicken meat with E. coli contaminant by using random forest and support vector machine, Biosens. Bioelectron. 9 (2021), 100083.
[51] V.A. Binson, M. Subramoniam, L. Mathew, Detection of COPD and Lung Cancer with electronic nose using ensemble learning methods, Clin. Chim. Acta 523 (2021) 231.